CHAPTER 5

ENDLESS LINEAR POLARIZATION PHASE SHIFTER

5.1. Introduction

Recently, the use of passive optical components like halfwave plate (HWP) and quarter-wave plate (QWP) in a polarization controller for coherent optical fiber communication systems has been proposed [86]. In such controller, they were operated as SOP transformers which transformed and arbitrary SOP of the signal light into a linear SOP matching that of the LO. An all fiber version of these phase plates consisting of two rotatable fiber cranks (FC) has also been reporte [83].

In this chapter, another application of these devices in phase shifting technique is presented. Previously, similar implementation using these phase plates in phase compensation interferometers have been reported [97-100]. However, the phase shifting method described here is intended for implementing in the polarization recombining scheme.

5.2. Principle

The HWP and QWP can be arranged in a variety of ways to form a phase shifter. In the present application, continuous phase shifting for linear polarization light is required, so two optical arrangements are considered; (1) use of two rotatable

and one stationary phase plates which is called Type-I phase shifter, and (2) use of one rotatable and two stationary phase plates which is called Type-II phase shifter.

5.2.1. Type-I phase shifter

The principle of operation for this type is illustrated in Fig. 37. The components of the device consist of a rotatable HWP, a rotatable QWP and a stationary QWP. Consider a vertically polarized light at A, its polarization plane can be rotated by rotating the HWP the rotation of which also induces optical phase shift to the input light. The first QWP then converts the linearly polarized light at B into a circularly polarized light at C by rotating this QWP twice the rotation angle of the HWP. Finally, a vertically or a horizontally polarized light at D can be obtained using the second QWP with its fast axis tilted either -45° or 45° to the x-axis, respectively.

To explain the action of this device mathematically, the Jones' polarization matrix calculus, which can describe passive optical components like HWP and QWP using the four element transformation matrix, is employed [101]. Let us assume a perfect HWP (phase retardation = π) and perfect QWP's (phase retardation = $\pi/2$). The transformation matrix M_H and M_{Qi} describing the phase retardation of the HWP and

the QWP's, respectively, in the x-y coordinates are given by

$$M_H = \begin{bmatrix} \cos\theta & -\sin\theta \\ \sin\theta & \cos\theta \end{bmatrix} \begin{bmatrix} e^{i\pi/2} & 0 \\ 0 & e^{-i\pi/2} \end{bmatrix} \begin{bmatrix} \cos\theta & \sin\theta \\ -\sin\theta & \cos\theta \end{bmatrix} \tag{56}$$

$$M_{Qi} = \begin{bmatrix} \cos\beta_i & -\sin\beta_i \\ \sin\beta_i & \cos\beta_i \end{bmatrix} \begin{bmatrix} e^{i\pi/4} & 0 \\ 0 & e^{-i\pi/4} \end{bmatrix} \begin{bmatrix} \cos\beta_i & \sin\beta_i \\ -\sin\beta_i & \cos\beta_i \end{bmatrix} \tag{57}$$

where, i = 1 for the rotatable QWP (FC2), and i = 2 for the stationary QWP (FC3). The last matrix on the right handside of eq.(56) transforms the input light to a coordinate system with its principal axes rotated by θ, the center matrix effects the phase retardation by π, and the first matrix causes a transformation back to the x-y coordinates. The same principle is also applied to eq.(57) but this time the principal axes of the input polarization is rotated by β, and the phase retardation is $\pi/2$.

With a vertical polarization input light of amplitude E_V and phase ϕ, we have for the complex vector electric field at A

$$E_A = E_V \begin{bmatrix} 0 \\ 1 \end{bmatrix} e^{i\phi} \tag{58}$$

and the complex vector electric field at D can be expressed as

$$E_D = M_{Q2}M_{Q1}M_H M_A \tag{59}$$

For a particular polarization state at D, let the HWP (FC1) rotated by α with respect to the x-axis in the clockwise direction, and the first QWP (FC2) rotated in the same direction with double rotation angle of the HWP such that its fast axis makes angle $\beta_1 = 2\alpha + 45°$ to the x-axis, and the second stationary QWP (FC3) tilted with its fast axis at $\beta_2 = 45°$ to the x-axis.

Insertion of eq.(56), eq.(57), and eq.(58) in eq.(59) for above condition gives

$$E_D = E_V \begin{bmatrix} \cos 2\alpha + i\sin 2\alpha \\ 0 \end{bmatrix} e^{i\phi}$$

$$= E_V \begin{bmatrix} 1 \\ 0 \end{bmatrix} e^{i(\phi + 2\alpha)} \tag{60}$$

From eq.(60) it can be seen that rotating the HWP by α and the QWP by 2α causes a 2α phase shift in the signal phase at D, without effecting its magnitude. In this arrangement, the second QWP transforms the input vertical polarization into the horizontal polarization at the output. This means that the phase shifter also operates as a 90° linear polarization rotator.

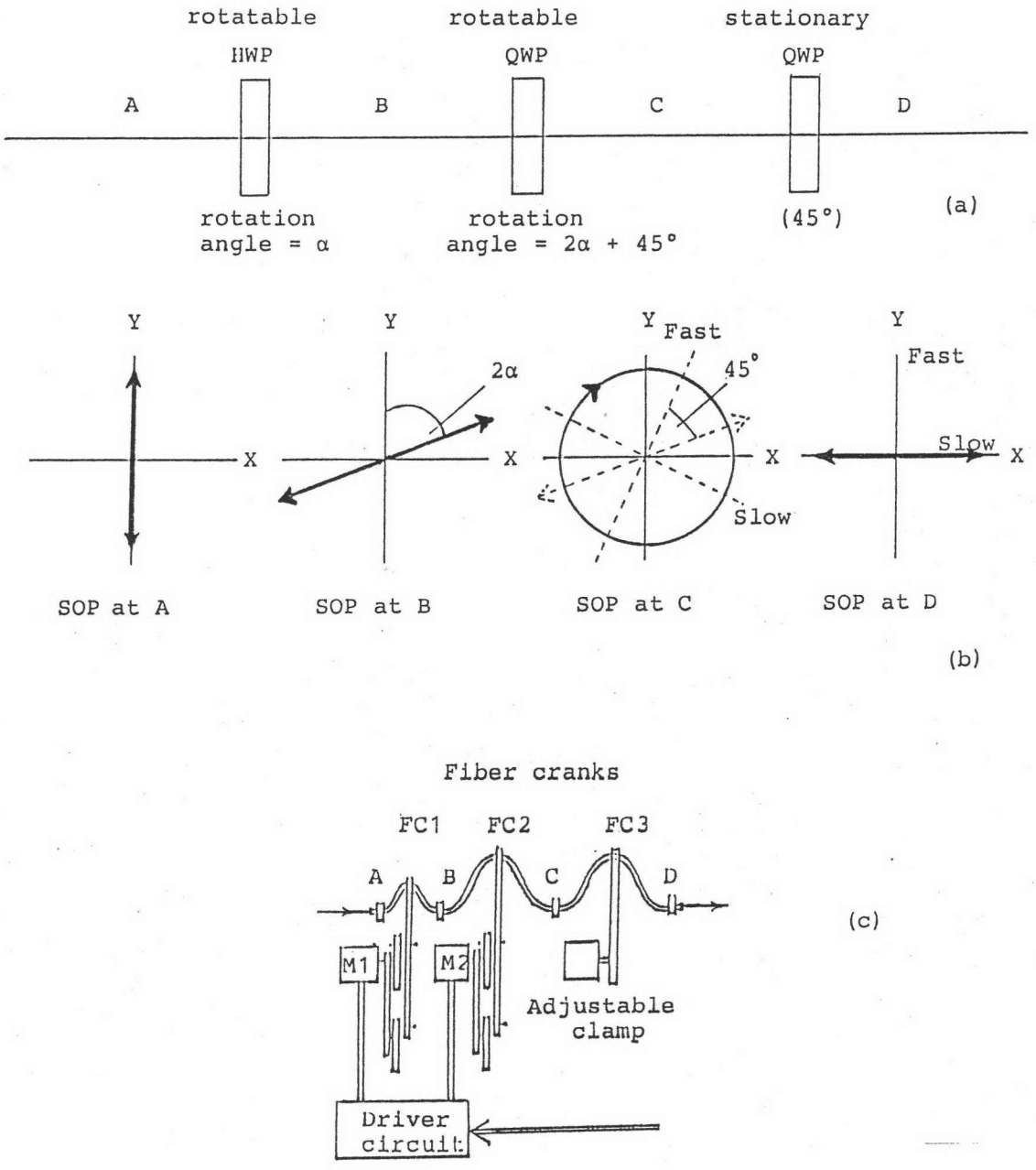

Fig. 37. Type-I endless phase shifter arrangement. HWP : half-wave plate; QWP : quarter-wave plate.

5.2.2. Type-II phase shifter

This type of phase shifter consists of a stationary QWP oriented at 45° to the x-axis, followed by a rotatable HWP, followed by a stationary QWP oriented at -45° to the x-axis, as shown in Fig. 38. The principle of the operation is as follows. A vertical linearly polarized input light is converted by the first QWP, into a left-handed circularly polarized light which is then converted into a right-handed circularly polarized light by the HWP rotated in the counterclockwise direction. The rotation of the HWP also causes an optical phase shift of two times its rotation angle. The successive QWP is used to convert the right-handed circularly polarized light back to a linearly polarized light (i.e. a horizontal linearly polarized light in this arrangement). Similarly, the Jones' polarization matrix calculus and complex wave representation as used in the analysis of the Type-I phase shifter can be applied here to explain the phase shifting function of the HWP.

Again, a perfect HWP (phase retardation = π) and perfect QWP's (phase retardation = $\pi/2$) are assumed. According to eq.(56) and eq.(57) the transformation matrix M_H of the HWP, the transformation matrix M_{Q1} of the 45°-oriented QWP, and the transformation matrix M_{Q2} of the -45°-oriented QWP, in the x-y coordinates, can be expressed as

$$M_H = -i\begin{bmatrix} \cos 2\alpha & \sin 2\alpha \\ \sin 2\alpha & -\cos 2\alpha \end{bmatrix} \tag{61}$$

$$M_{Q1} = \frac{1}{\sqrt{2}}\begin{bmatrix} 1 & -i \\ -i & 1 \end{bmatrix} \tag{62}$$

$$M_{Q2} = \frac{1}{\sqrt{2}}\begin{bmatrix} 1 & i \\ i & 1 \end{bmatrix} \tag{63}$$

where α is the angle between the fast axis of the HWP and the X-axis.

Consider at A, a vertical linearly polarized input light of amplitude E_V and phase ϕ, the complex electric field is represented by

$$E_A = E_V\begin{bmatrix} 0 \\ 1 \end{bmatrix} e^{i\phi} \tag{64}$$

Hence, the complex electric field at D is given by

$$E_D = M_{Q2}M_H M_{Q1}E_A \tag{65}$$

Substituting eq.(61)-eq.(64) in eq.(65) gives

$$E_D = -\begin{bmatrix} \cos 2\alpha + i\sin 2\alpha \\ 0 \end{bmatrix} E_V e^{i\phi}$$

$$= -\begin{bmatrix} 1 \\ 0 \end{bmatrix} E_V e^{i(\phi + 2\alpha)} \tag{66}$$

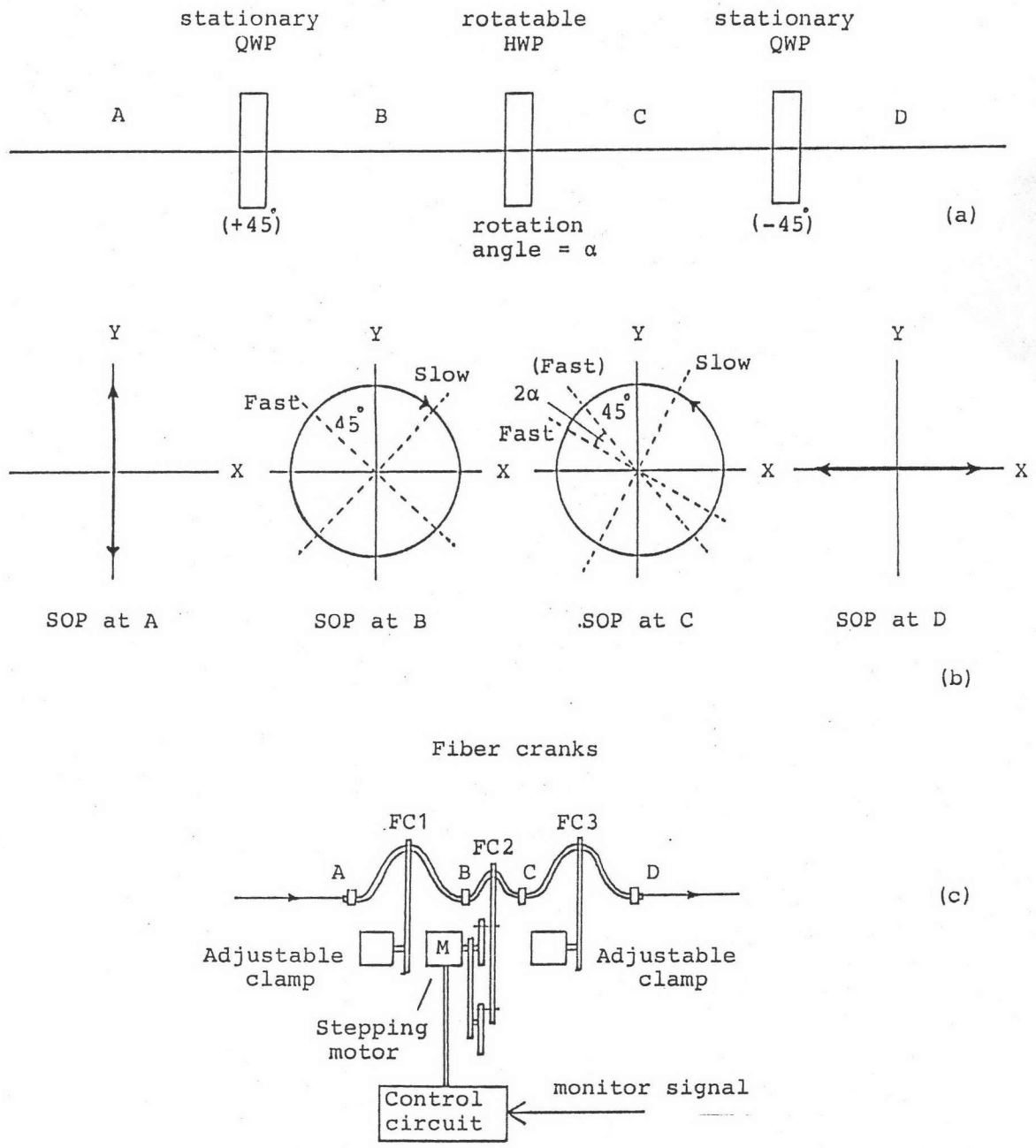

Fig. 38. Type-II endless plane shifter arrangement. HWP : half-wave plate; QWP : quarter-wave plate.

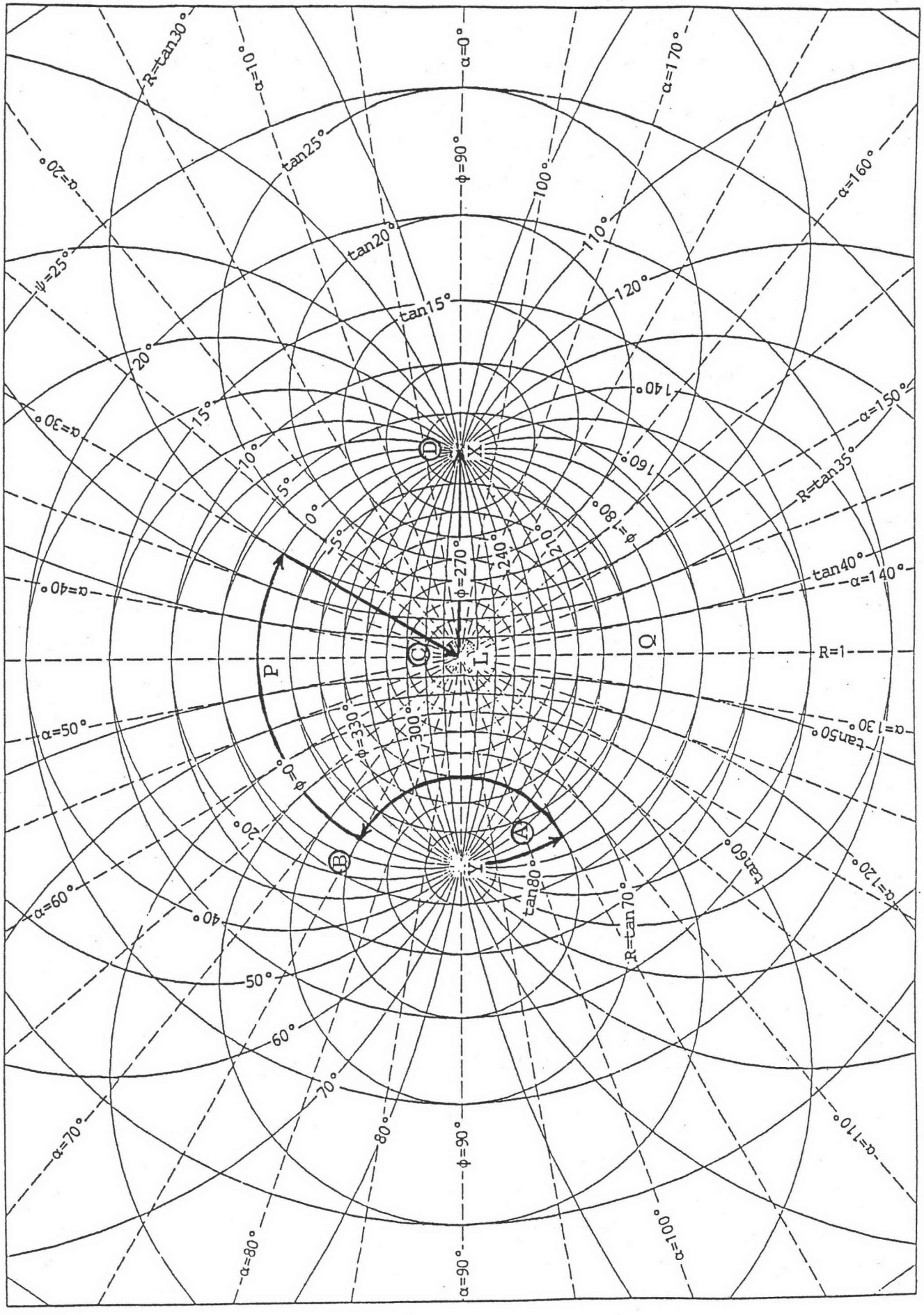

Fig. 39. A planar chart, illustrating sets of SOP's at different places (A, B, C, and D) along the path of the Type-I phase shifter.

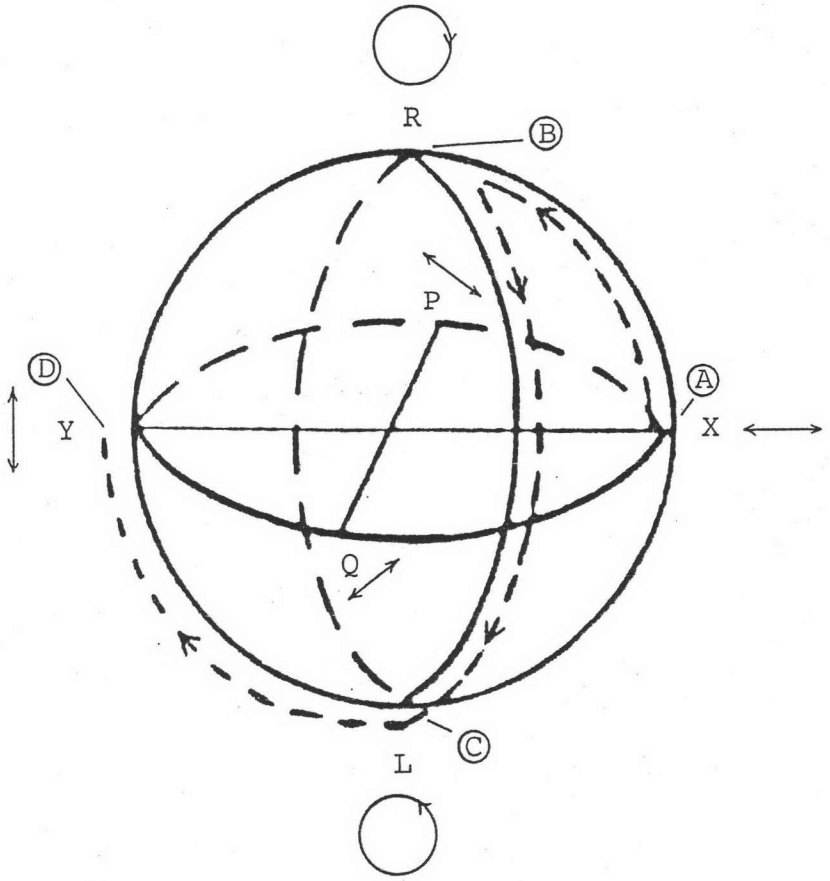

Fig. 40. Poincare sphere, illustrating sets of SOP's at different places (A, B, C, and D) along the path of the Type-II phase shifter.

where the resulting light is horizontal linearly polarized with an optical phase shift equal to 2α from the original phase but the amplitude is the same as that of the original input light at A. The above analysis also indicates that the optical arrangement in Fig. 38 operates as a 90° linearly polarization rotator as well.

For each type of phase shifters, evolutions of SOP at different points (A, B, C, and D) are illustrated in Fig. 39 (using a planar chart for Type-I phase shifters), and in Fig. 40 using Poincare sphere (for Type-II) respectively. In the experiment demonstration described in the next section, equivalent fiber crank configurations are used in place of the bulk optic phase plates.

5.3. Experimental verification

An automatic network analyzer has been developed to test the phase shifting property of the device, and apolarimeter consisting of rotating analyzers and QWP's which automatically measures the four Strokes parameters, is employed for polarization characteristics measurements. The experimental set up is shown in Fig. 41. Both output beams from a 1.35 μm DFB laser are utilized. One beam is frequency shifted by 100 MHz using an acousto-optic modulator before being splitted into two beams which are used as the LO

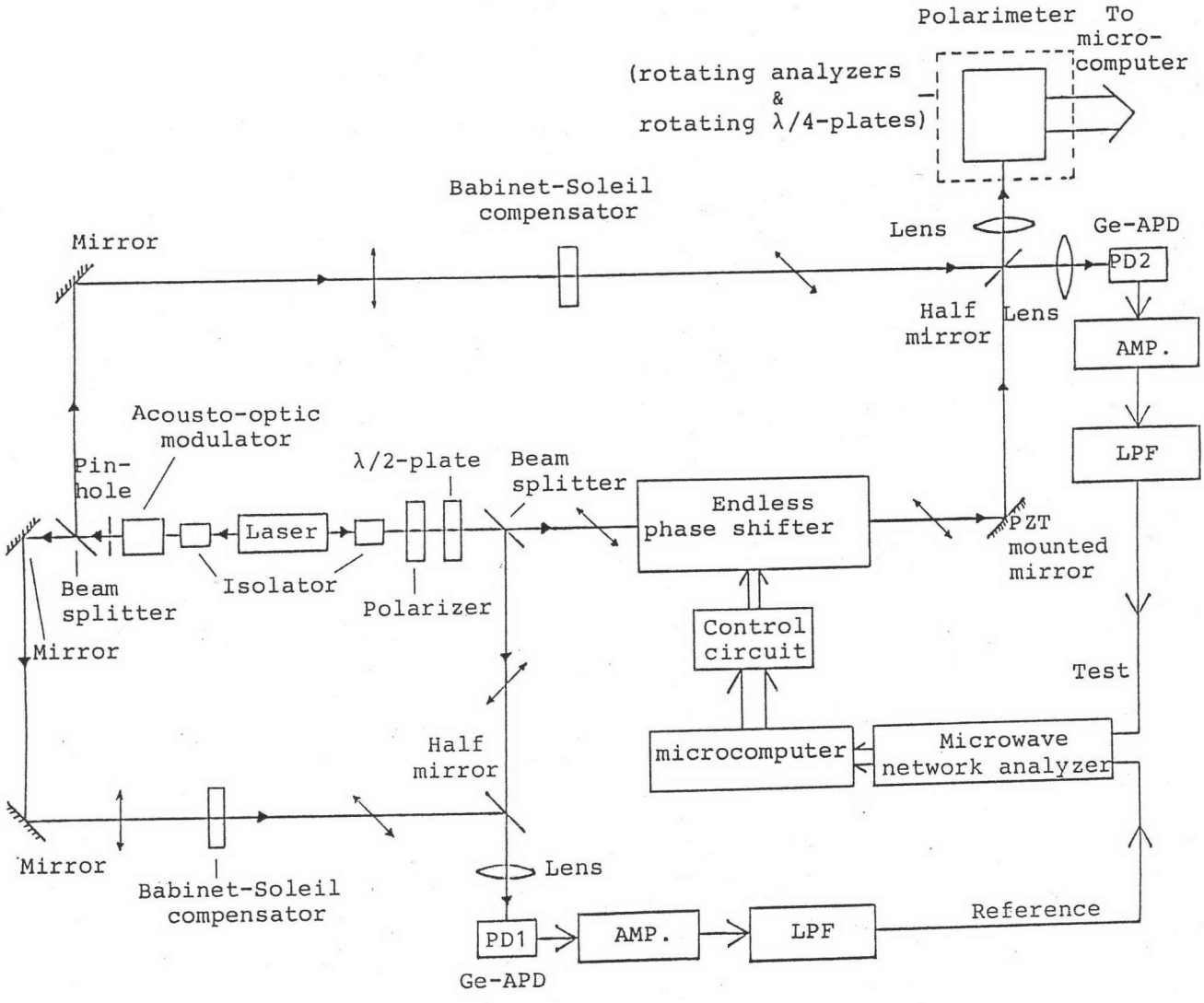

Fig. 41. Experimental setup for testing the properties and the polarization characteristics of the phase shifters.

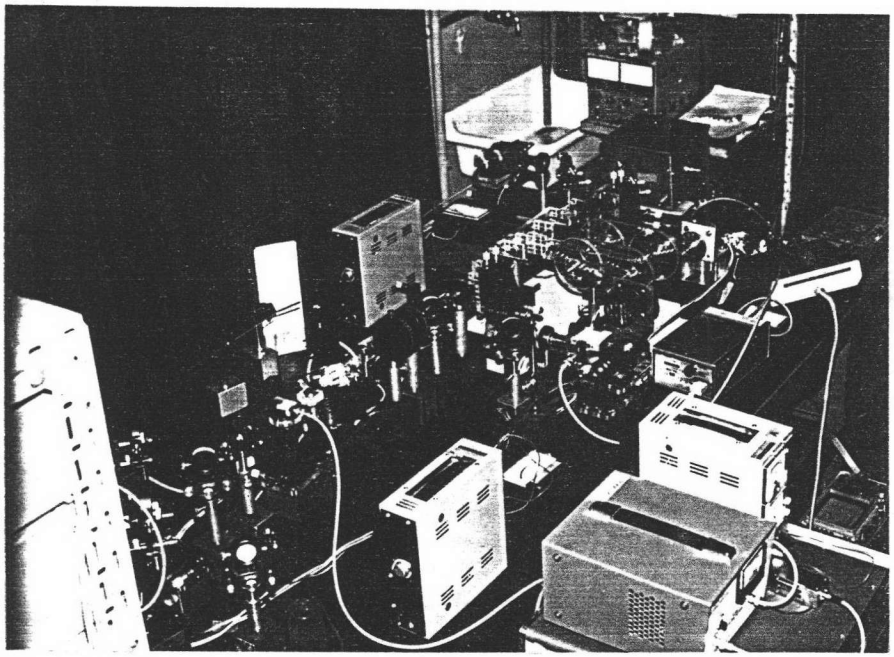

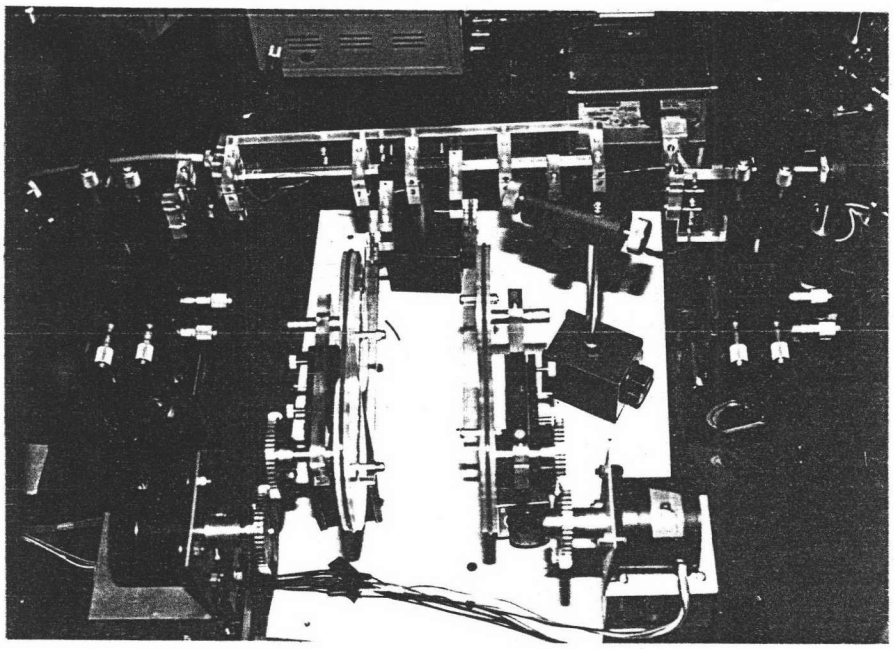

Photo. 2. Experimental setup for testing endless phase shifters.

ศูนย์วิทยทรัพยากร
จุฬาลงกรณ์มหาวิทยาลัย

beams. The other laser output beam is also splitted into two beams, on beam is launched into the fiber-crank phase shifter at -45° to the fiber (FC1) principal axis (x-axis) using polarizer and HWP, and is used as a test signal beam. The other beam is used as a reference signal beam. In order to permit the use of a commercially available network analyzer for measuring the relative phase and amplitude of these optical signals, heterodyne detections of the reference and signal beams are performed by mixing separately each of these beams with the LO beams. The mixed reference and test beams are then detected by the Ge-APD photodetectors PD1 and PD2, respectively, and then 100 MHz IF signals are analyzed by a Hewlett-Packard 8410A microwave network analyzer.

5.3.1. Results of Type-I phase shifter

Figure 42(a) and (b) show the results of phase and polar amplitude plots, respectively, as the fiber cranks FC1 and FC2 were continuously rotated every 0.25 second at 1.8° and 3.6°, respectively, for 10 minutes using stepping motors (M1, M2) controlled by a 4 Hz stepping pulse. It was found that a $2\alpha \pm 1°$ phase shift is obtained as the FC1 is rotated by α. $\pm 1°$ are possible due to the instrument error and mechanical disturbances. A circle shape is formed in the polar complex amplitude plot (Fig. 42(b)), indicating that

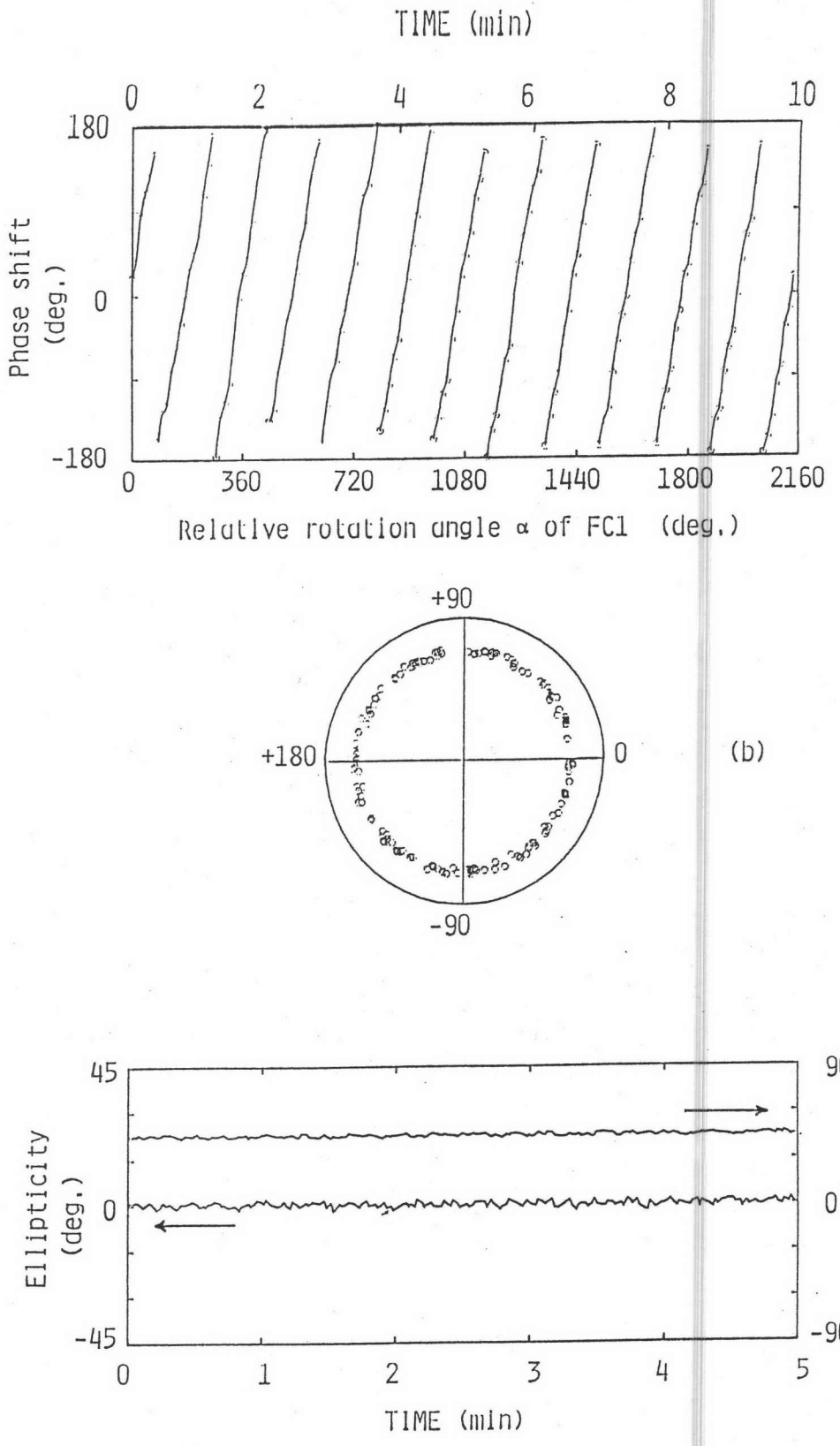

Fig. 42. Example of results of Type-I phase shifter: (a) relative phase shift as a function of FC1 rotation angle; (b) polar complex amplitude plot; (c) polarization characteristics.

the amplitude of the test signal is constant within the experimental error as the phase is swept through 360° many times. Polarization characteristics as shown in Fig. 42(c), are measured with the polarimeter by removing the half mirror in front of PD1 and detecting the FC output light directly, as the FC1 and FC2 are continuously rotated as before for 5 minutes. It is found that the SOP of the output light from the phase shifter is always linear with a fixed deflection angle (45° in this case). When rotating the FC3 by 90° in the counterclockwise direction, the initial deflection angle is preserved. The above results, clearly verify the principle operation of the proposed endless phase shifter.

5.3.2. Results of Type-II phase shifter

The Type-II phase shifter experiment, the results (see Fig.43) were found to be similar to those obtained with the Type-I. In Fig. 43(c), the deflection angle is 45° because all the polarization planes of the lights in Fig. 40 have been rotated by 90°. It was also found that rotating the HWP by α causing a $2\alpha \pm 1°$ phase shift in the signal phase in good agreement with the theory.

5.4. Error analysis

In practice, the phase retardation of the HWP and

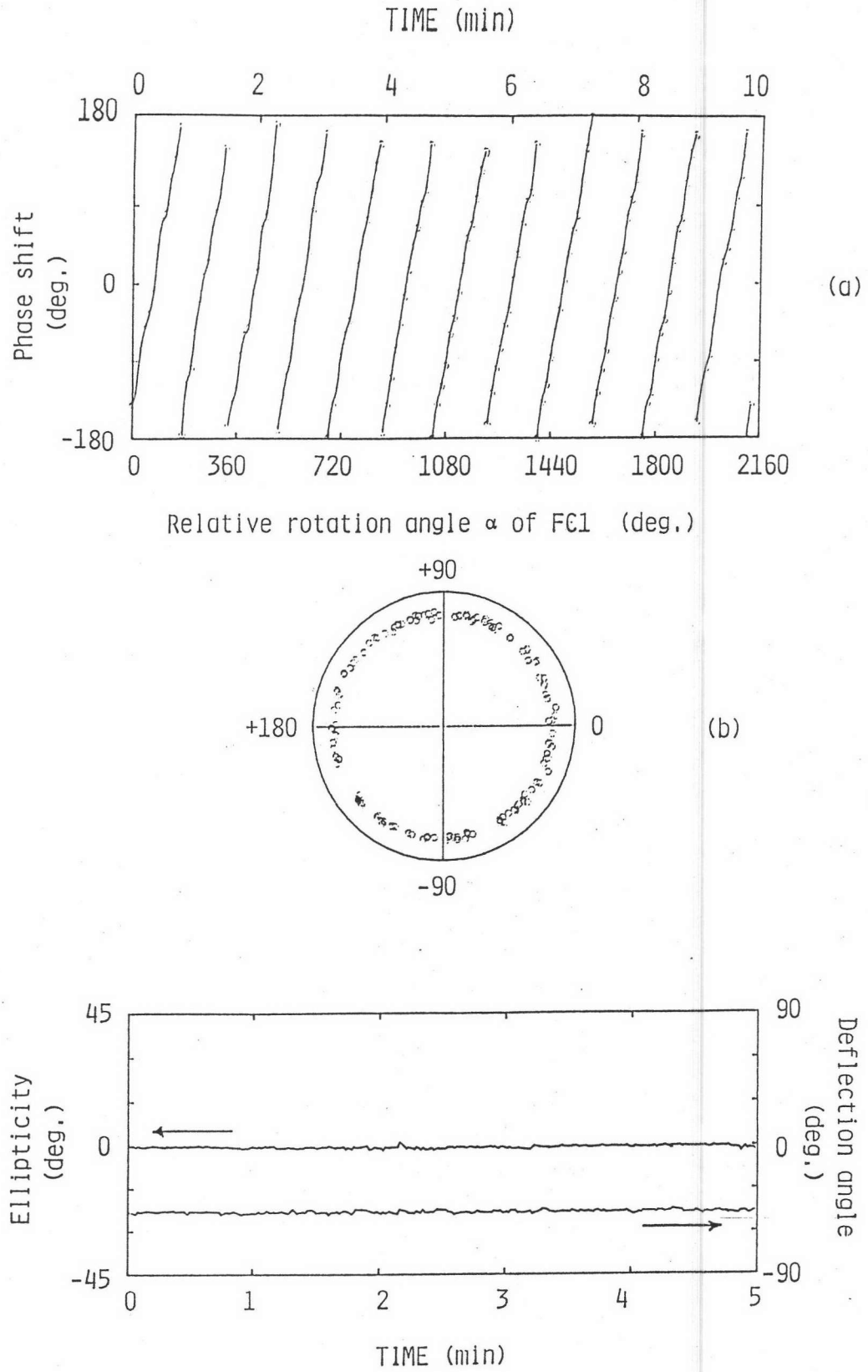

Fig. 43. Example of results of Type-II phase shifter: (a) relative phase shifter as a function of FC1 rotation angle; (b) polar complex amplitude plot; (c) polarization characteristics.

QWP are not exactly equal to π and $\pi/2$, respectively. Therefore, it is important to determine the effect of the imperfect phase plates on the power factor ($10*\log(I_1/(I_1 + I_2))$) or the extinction ratio ($10*\log(I_1/I_2)$) of the polarization recombining output intensities. We analize here, the error due to imperfect phase plates in the Type-II phase shifter.

According to eq.(56), transformation matrix for general phase plate can be expressed as

$$M_{general} = \begin{bmatrix} \cos(\delta/2)+j\cos2\theta\sin(\delta/2) & j\sin2\theta\sin(\delta/2) \\ j\sin2\theta\sin(\delta/2) & \cos(\delta/2)-j\cos2\theta\sin(\delta/2) \end{bmatrix} \quad (67)$$

where θ is the angle of the principal axis (fast axis) of a phase plate tilted with respect to the x-axis, and δ represents retardation of such phase plate.

For perfect phase plates :

$\theta = \alpha$, $\delta = \pi$, for HWP

$\theta = 45°$, $\delta = \pi/2$, for QWP1

$\theta = -45°$, $\delta = \pi/2$, for QWP2

For imperfect phase plates :

$\theta = \alpha$, $\delta = \pi + \varepsilon_H$, for HWP

$\theta = 45°$, $\delta = \pi/2 + \varepsilon_Q$, for QWP1

$\theta = -45°$, $\delta = \pi/2 + \varepsilon_Q$, for QWP2

Assuming that the tilt angle of the QWP's are perfectly aligned with respect to the x-axis, and the two QWP's have the same property. ε is the phase error due to imperfect phase retardation.

Using eq.(67), the transformation matrices for imperfect HWP and QWP's can be expressed as

$$M^{\varepsilon}_{H} = \begin{bmatrix} \cos(\delta_H/2)+j\cos2\alpha\sin(\delta_H/2) & j\sin2\alpha\sin(\delta_H/2) \\ j\sin2\alpha\sin(\delta_H/2) & \cos(\delta_H/2)-j\cos2\alpha\sin(\delta_H/2) \end{bmatrix} \tag{68}$$

$$M^{\varepsilon}_{Q1} = \begin{bmatrix} \cos(\delta_Q/2) & j\sin(\delta_Q/2) \\ j\sin(\delta_Q/2) & \cos(\delta_Q/2) \end{bmatrix} \tag{69}$$

$$M^{\varepsilon}_{Q2} = \begin{bmatrix} \cos(\delta_Q/2) & -j\sin(\delta_Q/2) \\ -j\sin(\delta_Q/2) & \cos(\delta_Q/2) \end{bmatrix} \tag{70}$$

Consider a vertical polarization input light of amplitude E_V and phase ϕ_V, as before the complex vector electric field at A is given by

$$E_A = E_V \begin{bmatrix} 0 \\ 1 \end{bmatrix} e^{j\phi_V} \tag{71}$$

and the complex vector electric field at D can be expressed as

$$\begin{aligned} E_D &= M^{\varepsilon}_{Q2} M^{\varepsilon}_{H} M^{\varepsilon}_{Q1} E_A \\ &= E_V \begin{bmatrix} -\cos2\alpha\cos(\delta_H/2)\cos(\varepsilon_Q) + j\sin2\alpha\cos(\varepsilon_H/2) \\ -\sin(\varepsilon_H/2) + j\cos2\alpha\cos(\varepsilon_H/2)\sin(\varepsilon_Q) \end{bmatrix} e^{j\phi_V} \end{aligned} \tag{72}$$

When $\varepsilon_H = \varepsilon_Q = 0$, eq.(72) reduces to eq.(66) i.e. in the case of perfect phase plates.

Now let consider the interference between the electric fields in Fig. 44. The electric field in branch 1 is expressed as

$$E_1 = E_H \begin{bmatrix} 1 \\ 0 \end{bmatrix} e^{j\phi_H} \tag{73}$$

where E_H and ϕ_H are the amplitude and phase of the H: component, respectively.

The electric field in branch 2 is given by

$$E_2 = E_D \tag{74}$$

The interference outputs E_3 and E_4 at output ports 3 and 4, respectively, are expressed as

$$E_3 = E_1 + E_2 \tag{75}$$

$$E_4 = E_1 - E_2 \tag{76}$$

and the corresponding photocurrents I_3 and I_4 are

$$\begin{aligned} I_3 &= E_3 . E_3^* \\ &= E_H^2 + E_V^2 + E_H E_V \{ \\ &\quad \cos(\varepsilon_H/2)\cos\varepsilon_Q[\cos(\phi_H-\phi_V+2\alpha)+\cos(\phi_H-\phi_V-2\alpha)] \\ &\quad + \cos(\varepsilon_H/2)[\cos(\phi_H-\phi_V-2\alpha)-\cos(\phi_H-\phi_V+2\alpha)]\} \end{aligned} \tag{77}$$

$$\begin{aligned} I_4 &= E_4 . E_4^* \\ &= E_H^2 + E_V^2 - E_H E_V \{ \\ &\quad \cos(\varepsilon_H/2)\cos\varepsilon_Q[\cos(\phi_H-\phi_V+2\alpha)+\cos(\phi_H-\phi_V-2\alpha)] \\ &\quad + \cos(\varepsilon_H/2)[\cos(\phi_H-\phi_V-2\alpha)-\cos(\phi_H-\phi_V+2\alpha)]\} \end{aligned} \tag{78}$$

For $\varepsilon_H = \varepsilon_Q = 0$, eq.(77) and eq.(78) reduce to

$$I_3 = E_H^2 + E_V^2 + 2E_HE_V\cos(\phi_H-\phi_V-2\alpha) \tag{79}$$

$$I_4 = E_H^2 + E_V^2 - 2E_HE_V\cos(\phi_H-\phi_V-2\alpha) \tag{80}$$

which are equivalent to eq.(34) and eq.(35) for the ideal case.

For simplicity, we further assume that $E_H = E_V$, eq.(77) and eq.(78) become

$$I_3 = E_H^2\{2 + \cos(\varepsilon_H/2)\cos\varepsilon_Q[\cos4\alpha + 1] + \cos(\varepsilon_H/2)[1 - \cos4\alpha]\} \tag{81}$$

$$I_4 = E_H^2\{2 - \cos(\varepsilon_H/2)\cos\varepsilon_Q[\cos4\alpha + 1] - \cos(\varepsilon_H/2)[1 - \cos4\alpha]\} \tag{82}$$

The power factor η is defined as

$$\eta = 10*\log(I_3/(I_3 + I_4)) \tag{83}$$

The plot of the power factor as a function of HWP rotation angle α, with ε_H and ε_Q are the parameters, is shown in Fig. 45. It is found that for $1° < \varepsilon_H, \varepsilon_Q < 5°$ the power factor is degraded only within 0.01 dB. The HWP's and QWP's available on the market exhibit values of ε_H and ε_Q from $\lambda/20$ (mica) to $\lambda/500$ (quartz). Therefore, with the present phase plate quality, the power factor degradation within 0.01 dB can be readily achieved in practice. This value is very small and

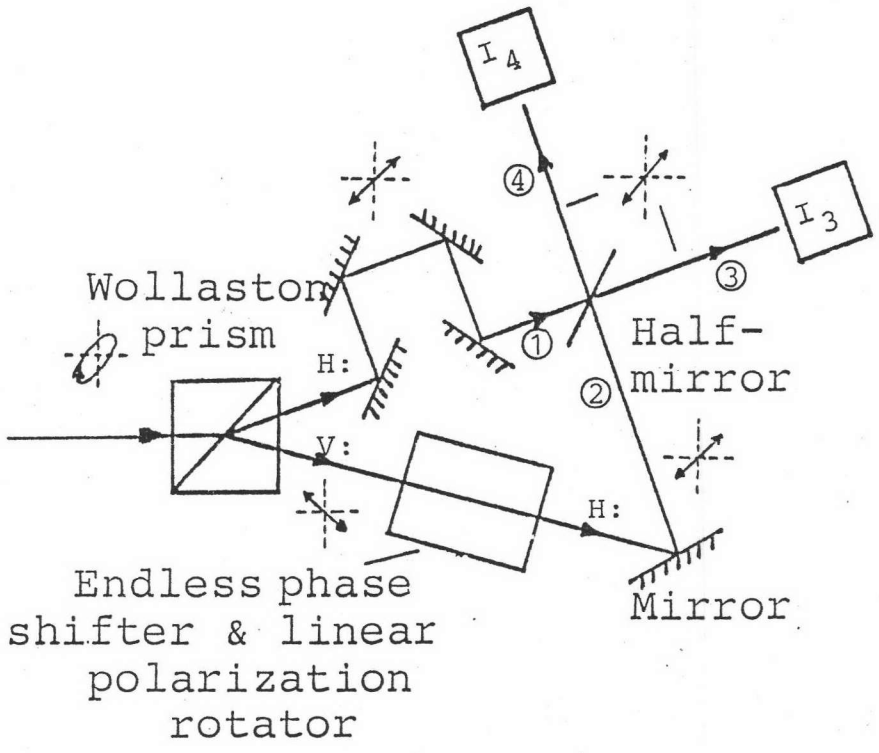

Fig. 44. Schematic diagram of polarization recombining scheme with endless phase shifter and 90° linear polarization rotator.

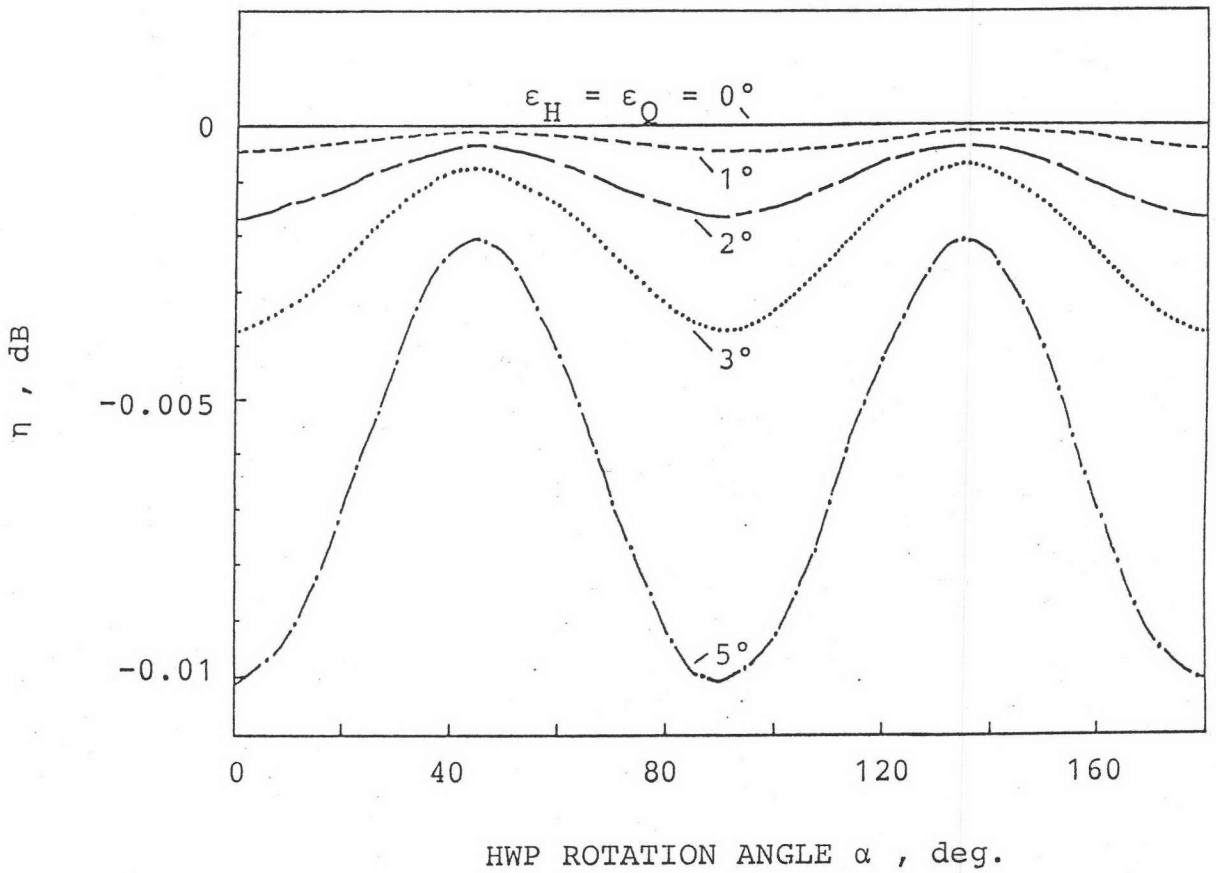

Fig. 45. Power factor η as a function of HWP rotation angle α with imperfect phase plates. ε_H : HWP phase retardation error; ε_Q :QWP phase retardation error.

negligible compared with other means of power loss (e.g. insertion loss). As far as the tilted angle misalignement is concerned, angle of 45° between the principal axes of the QWPs and the x-axis can be obtained with sufficient accuracy. The above analysis also applies to the equivalent fiber-crank configurations used in the experiments.

The results obtained with these devices were consistent with the phase plate specification, and indicated that they had been properly constructed.

5.5. Summary

Two types of endless phase shifter based on simple polarization rotating techniques are described and tested. These devices can also be used as a 90° linear polarization rotator. Error due to imperfect phase retardations can be neglected considering the property of the commercial available phase plates.